



Galactic Chemical Evolution of Exoplanet Hosting Stars: Are High-mass Planetary Systems Young?

C. Swastik^{1,2}, Ravinder K. Banyal¹, Mayank Narang³, P. Manoj³, T. Sivaramani¹, S. P. Rajaguru¹, Athira Unni^{1,2}, and Bihan Banerjee³

¹Indian Institute of Astrophysics, Koramangala 2nd Block, Bangalore 560034, India; swastik.chowbay@iiap.res.in

²Pondicherry University, R.V. Nagar, Kalapet, 605014, Puducherry, India

³Department of Astronomy and Astrophysics, Tata Institute of Fundamental Research Homi Bhabha Road, Colaba, Mumbai 400005, India

Received 2022 April 18; revised 2022 May 29; accepted 2022 May 31; published 2022 July 19

Abstract

The imprints of stellar nucleosynthesis and chemical evolution of the galaxy can be seen in different stellar populations, with older generation stars showing higher α -element abundances and the later generations becoming enriched with iron-peak elements. The evolutionary connections and chemical characteristics of circumstellar disks, stars, and their planetary companions can be inferred by studying the interdependence of planetary and host star properties. Numerous studies in the past have confirmed that high-mass giant planets are commonly found around metal-rich stars, while the stellar hosts of low-mass planets have a wide range of metallicity. In this work, we analyzed the detailed chemical abundances for a sample of >900 exoplanet hosting stars drawn from different radial velocity and transit surveys. We correlate the stellar abundance trends for α - and iron-peak elements with the planets' mass. We find the planet mass–abundance correlation to be primarily negative for α -elements and marginally positive or zero for the iron-peak elements, indicating that stars hosting giant planets are relatively younger. This is further validated by the age of the host stars obtained from isochrone fitting. The later enrichment of protoplanetary material with iron and iron-peak elements is also consistent with the formation of the giant planets via the core accretion process. A higher metal fraction in the protoplanetary disk is conducive to rapid core growth, thus providing a plausible route for the formation of giant planets. This study, therefore, indicates that the observed trends in stellar abundances and planet mass are most likely a natural consequence of Galactic chemical evolution.

Unified Astronomy Thesaurus concepts: [Spectroscopy \(1558\)](#); [Extrasolar gaseous giant planets \(509\)](#); [Exoplanet formation \(492\)](#); [Stellar ages \(1581\)](#); [Metallicity \(1031\)](#); [Chemical abundances \(224\)](#); [Exoplanets \(498\)](#)

Supporting material: machine-readable table

1. Introduction

When, where, and how planets are formed is an actively pursued area in exoplanet science. Ever since the discovery of the first exoplanet 51 Peg by Mayor and Queloz (Mayor & Queloz 1995), the field of exoplanets has been rapidly growing. With planetary census already reaching the 5000 mark, it becomes statistically feasible to study the properties of the planets and their host stars to address various scientific goals. At a broader level, one such goal is to understand how fundamental properties (e.g., age, mass, chemical composition, T_{eff} , $\log g$) of stars hosting planets differ from stars without planets (SWPs). Further insights can be gained by correlating various astrophysical properties of stellar hosts with the orbital and physical properties of the exoplanets occupying a wide parameter space.

The early detections using radial velocity (RV) techniques have shown that the occurrence of Jupiter-like planets is higher around metal-rich stars (e.g., Gonzalez 1997; Santos et al. 2001; Fischer & Valenti 2005; Udry & Santos 2007). Subsequently, extensive spectroscopic surveys of planet hosts (e.g., Bruntt et al. 2012; Everett et al. 2013; Buchhave et al. 2014; Dong et al. 2014; Fleming et al. 2015; Johnson et al. 2017; Mulders 2018;

Narang et al. 2018; Petigura et al. 2018; Swastik et al. 2021) have shown that (a) host star metallicity ($[\text{Fe}/\text{H}]$) increases as a function of planet mass, peaking around $M_p \approx 4 M_J$ and showing large scatter for the massive giant planets and brown dwarf hosts (Narang et al. 2018; Swastik et al. 2021); and (b) overall stars with planets tend to have higher metallicity than SWPs. Two main theories have been put forward to explain this metallicity excess (Ecuvillon et al. 2004). The “primordial” hypothesis suggested that the initial protoplanetary cloud was metal-rich, which resulted in such metal-rich hosts (Santos et al. 2004; Valenti & Fischer 2008; Johnson et al. 2010a). On the other hand, the “self-enrichment” hypothesis attributed the high-metallicity content of the planet-bearing stars to the accretion of a large amount of rocky and metal-rich planets (Lin et al. 1996; Laughlin & Adams 1997; Gonzalez 1997; Murray et al. 2001; Pinsonneault et al. 2001). Regardless of the validity of one theory or another, the growing consensus is that a metal-rich environment plays a vital role in forming planetary systems. Particularly, the gas giants are believed to be formed from the core accretion process, which requires fast buildup of the planetary core up to $10\text{--}15 M_{\oplus}$. The core has to be formed quickly within a few Myr before the gas in the disk dissipates. The metal-rich protoplanetary material aids the formation of the cores followed by the accretion of the gas to form the outer envelope.



Original content from this work may be used under the terms of the [Creative Commons Attribution 4.0 licence](#). Any further distribution of this work must maintain attribution to the author(s) and the title of the work, journal citation and DOI.

In the context of planet formation, most of the aforementioned studies have mainly focused on iron abundances ([Fe/H]). It is also because estimating the abundances of all the elements for a given star is not always straightforward. Although iron is not the most abundant metal in the universe, the optical spectra for the solar-type stars contain many prominent iron lines, making the abundance determination easier (Blanco-Cuaresma et al. 2014; Adibekyan 2019). The iron abundance is also traditionally used as a proxy for overall metallicity of the star with the assumption that the composition of the metals changes proportionally to the iron content. However, the formation mechanism for different elements is vastly different, and their signatures do show up in the chemical composition of stars. Therefore, studying stars' detailed abundance patterns could provide further clues to the observed planet morphology and architecture.

In the past, there have been limited studies of elemental abundances, i.e., $[X/Fe]$ for a larger sample of planet-hosting stars (PHSs). For example, Brugamyer et al. (2011), Adibekyan et al. (2012a), Hinkel et al. (2014), Brewer et al. (2016), and Brewer & Fischer (2018) analyzed the spectra of known planetary hosts and found an overabundance of α -elements (Mg, Si, S, Ca, Ti) for the PHSs. Similarly, Delgado Mena et al. (2017) and Delgado Mena et al. (2018) investigated the abundances of heavy elements of PHSs and found that stars with planets show an overabundance of elements such as Zn for $[Fe/H] < -0.1$ dex. They also found most s -process elements to be underabundant in PHSs. These studies clearly show that knowing iron content of stars alone is not sufficient, and a detailed abundance analysis is required to understand the complete picture of planet formation. The limited studies that focused on the $[X/Fe]$ were mainly based on specific elements (such as only on α - or iron-peak elements). Similarly, studies such as Wilson et al. (2022) investigated the correlation between occurrence rate and chemical abundances for 10 elements for the host stars of Kepler planets. They also studied the correlation between planet radius (R_p) and abundances and detected a significant correlation between $[Mn/Fe]$ and R_p . However, these results are highly skewed toward shorter orbital period planets. A recent investigation by Tautvaišienė & Mikolaitis (2022) focused on 25 RV-detected PHSs and found that main-sequence giant PHSs are metal-rich compared to the low-mass PHSs. They also found that PHSs are systematically higher in α -content than the nonhosting counterparts at the lower-metallicity regime ($[Fe/H] \leq -0.2$). These studies provide scientific motivation for us to investigate how the planet mass M_p varies as a function of the abundances of different classes of elements and for a diverse sample of PHSs detected by both transit and RV. Studying the $[X/Fe]$ pattern with M_p can also give clues about the preferred formation route for planets belonging to different mass ranges.

In the context of the standard galactic chemical evolution (GCE), core-collapse supernovae (SNe), mostly Type II (SNe II), enriched the early universe with α -elements, which also occurred on a faster timescale than Type Ia SNe (SNe Ia; Matteucci & Francois 1989; Alibés et al. 2001; Matteucci et al. 2009; Kobayashi et al. 2020). According to the classical view, an SN II occurs when a massive star collapses ($M_* > 8M_\odot$) rapidly after the completion of its stellar burning process, which ends in an explosion. On the other hand, the most accepted model of SNe Ia involves a binary system in which at least one of the stars is a white dwarf. The white dwarf accretes

mass from its binary companion and reaches the critical mass (also known as the Chandrasekhar limit), which results in thermal runaway, followed by an explosion. The SNe II produce a large amount of α -elements and fewer iron-peak elements. The SNe Ia, on the other hand, are the major producer of iron-peak elements (Edvardsson et al. 1993; Costa Silva et al. 2020; Kobayashi et al. 2020). As a consequence of staggered progression, iron-peak elements enriched the interstellar medium (ISM) at a much later stage compared to the α -elements. Therefore, at the population level, the α to iron-peak ratio, $[\alpha/Fe]$, in stars is a good proxy for age to probe the history of GCE (Haywood et al. 2013; Delgado Mena et al. 2019; Costa Silva et al. 2020; Kobayashi et al. 2020).

In this paper, we study the elemental abundances of a large sample of over 900 PHSs with the goal of examining the role of GCE in the context of exoplanetary systems. We infer that the majority of the high-mass planetary systems ($M_p > 0.3 M_J$) are likely formed at later stages of the GCE, mainly after SNe Ia have sufficiently enriched the Galactic ISM with iron-peak elements. Our premise is based on the fact that production of most elements is dictated by GCE and a heavy-element-driven core accretion mechanism is a favored pathway for the formation of giant planets. Further motivation for this work has come from a recent study of stellar kinematics of PHSs by Narang et al. 2022 (under review), suggesting that the host stars of Jupiter-type planets have a smaller velocity dispersion, which is attributed to their relatively young age.

For this work, we use the spectroscopic abundances of PHSs obtained from three previous studies, namely, HARPS-GTO (Mayor et al. 2003; Lo Curto et al. 2010; Santos et al. 2011), California Kepler Survey (CKS; Brewer & Fischer 2018), and California Planet Survey (CPS; Brewer et al. 2016). We measured the correlation between $[X/Fe]$ and planet mass to statistically examine whether stars hosting giant planets are younger than the small planet hosts. We interpret our results in terms of GCE and mainly focus on the α - and iron-peak elements since their formation time line is evidently different. In our findings, α -elements and Eu show a strong negative correlation with planet mass, but not so significant correlation was found for the iron-peak and s -process elements.

The rest of the paper is organized as follows. In Section 2, we describe our sample. In Section 3, we discuss the various $[X/Fe]$ trends as a function of planet mass. Further, in Section 4, we compare the trends obtained in Section 3 and interpret our results. Finally, we give our summary and conclusions in Section 5.

2. Sample Preparation

To study the elemental abundances of the α -, iron-peak, and other elements (mainly the s -process and r -process elements) of the exoplanet host stars, we used the data set from three different surveys, namely, HARPS-GTO (Mayor et al. 2003; Lo Curto et al. 2010; Santos et al. 2011), CPS (Brewer et al. 2016), and CKS (Brewer & Fischer 2018). The plot between T_{eff} and $\log g$ for the stars combined from the above three samples is shown in Figure 1. In this work, we analyze the main-sequence stars that lie below the dashed black line shown in Figure 1. We divided the planet masses taken from NASA's exoplanet archive into three mass bins, namely, small planets (SP; $M_p \leq 0.3 M_J$), giant planets (GP; $0.3 M_J < M_p \leq 4 M_J$), and super-Jupiters (SJ; $4 M_J < M_p \leq 13 M_J$). In this section, we

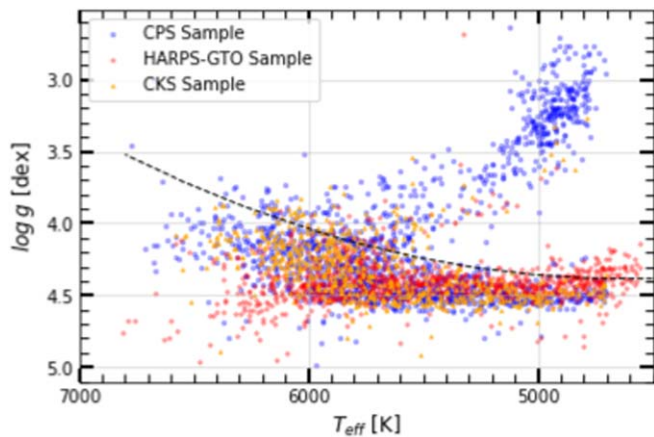


Figure 1. Exoplanet host stars from the HARPS-GTO (red), CPS (blue), and CKS (yellow) surveys. The dashed black line separates the main-sequence stars lying below the line from the evolved stars lying above (Brewer & Fischer 2018). In this paper, we study only the main-sequence stars.

briefly describe the original sample and how it was curated to obtain the final sample for our analysis.

2.1. HARPS-GTO Sample

The HARPS-GTO stars used in this study come from three HARPS subsamples: Mayor et al. (2003), Lo Curto et al. (2010), and Santos et al. (2011). The sample consists of 1111 F, G, and K main-sequence stars (Adibekyan et al. 2012b) observed with HARPS, a high-resolution spectrograph ($R \sim 115,000$) at the La Silla Observatory (ESO, Chile). The HARPS-GTO sample has 163 stars with at least one companion⁴ and 948 stars without any companion. The stars were extensively studied, and their chemical abundances are published in a series of papers (Adibekyan et al. 2011; Mayor et al. 2011; Adibekyan et al. 2012b; Bertran de Lis et al. 2015; Suárez-Andrés et al. 2016, 2017; Delgado Mena et al. 2017, 2018, 2019; Costa Silva et al. 2020; Delgado Mena et al. 2021). The technique employed to obtain the elemental abundances is mostly the equivalent width method. Initial study for the HARPS sample was done for elements with $A < 29$ by Adibekyan et al. (2012b), which focused mainly on chemical separation of thin- and thick-disk stars. The study also showed an overabundance of all the elements ($[X/H]$) for the giant planet hosts. However, no trends for $[X/Fe]$ with planet mass were studied. We took the elemental abundance of eight elements (Mg, Si, Ca, Ti, Cr, Ni, Co, Mn) from Adibekyan et al. (2012b) for our analysis.

For the neutron-capture elements, a separate study was conducted for the HARPS-GTO sample by Delgado Mena et al. (2017) and Delgado Mena et al. (2018). For the *s*-process such as Ba, Sr, Ce, and Zr, it is found that PHSs are underabundant compared to stars without a planetary companion. These results are significant, as they throw light on how *s*-process elemental abundances play a role in distinguishing stars with planets and SWPs. However, the stellar abundances as a function of planet mass were not studied in detail in these papers. Thus, we took the elemental abundances ($[X/Fe]$) for two iron-peak elements (Cu and Zn) and seven neutron-capture elements (Sr, Y, Zr, Ba, Ce, Nd, and Eu) from Delgado Mena et al. (2017) and combined them with the eight elements from

⁴ Data from <https://exoplanetarchive.ipac.caltech.edu/>.

Adibekyan et al. (2012b) to study the trends of α -, iron-peak, and *s*- and *r*-process elements as a function of planet mass.

2.2. California Planet Survey

The abundance of stars in CPS is taken from Brewer et al. (2016). The sample consists of 1615 F, G, K, and M stars that were observed using the HIRES spectrograph ($R \sim 70,000$) on the KECK I telescope as a part of the RV planet search program (Howard et al. 2010; Johnson et al. 2010b; Wright et al. 2011; Brewer et al. 2016). These stars were observed in the red configuration of HIRES without iodine cells in the beam path. We used the abundances of nine elements (Mg, Si, Ca, Ti, Cr, Mn, Fe, Ni, and Y) for our analysis from the CPS sample, which was obtained using the synthetic spectral fitting (Brewer et al. 2016; spectroscopy made easy (SME); Piskunov & Valenti 2017). To extract the PHSs from the sample, we cross-matched the CPS catalog with the NASA exoplanet archive (Akeson et al. 2013; NASA Exoplanet Science Institute 2020) with a search radius of $3''$ (see Viswanath et al. 2020 for details)⁵ and found that there are 227 stars hosting 361 planets.

2.3. California Kepler Survey

The CKS sample used in this study comes from Brewer & Fischer (2018). It consists of 1127 stars that are Kepler objects of interest (KOIs). The CKS sample primarily consists of KOIs with the magnitude in the Kepler band $K_p \leq 14.2$ (Borucki et al. 2011; Petigura et al. 2017; Johnson et al. 2017). The CKS KOIs used in this study were observed using the same instrumental configuration as that of the CPS host stars described in Section 2.2. For our analysis, we took the elemental abundances for nine elements (Mg, Si, Ca, Ti, Cr, Mn, Fe, Ni, and Y) for the KOIs from Brewer & Fischer (2018), which used synthetic spectral fitting similar to the CPS host stars. We cross-matched the CKS data used in this study with the NASA exoplanet archive (Akeson et al. 2013; NASA Exoplanet Science Institute 2020) with a search radius of $3''$ (same as done for CPS) and found a total of 600 stars hosting at least one planet. The remainder of the sample consists of planetary candidates, false positives, and SWPs (see the [kepler false-positive table](#) for details). For our analysis, we have only considered the main-sequence stars from the CKS sample, which hosts confirmed planets.

2.4. Planet Mass

The data for the planet mass were mostly obtained from the NASA exoplanet archive (Akeson et al. 2013; NASA Exoplanet Science Institute 2020). For 24 planets, the masses were taken from the exoplanet.eu catalog for which the mass was not available in the NASA exoplanet archive. For the transiting planets in the CKS sample, the mass is derived from the mass–radius relation given by Chen & Kipping (2017). For planets detected by RV in the HARPS-GTO and CPS, the minimum mass (M_P) was used. For the giant planets in the CKS sample for which the RV follow-up observations were done, the actual mass derived from the RV analysis was used.

⁵ We used a larger search radius initially but found that a search radius of $3''$ was sufficient in this case to extract all the PHSs. We also double-checked them with other parameters such as SIMBAD name to verify that they are truly PHSs.

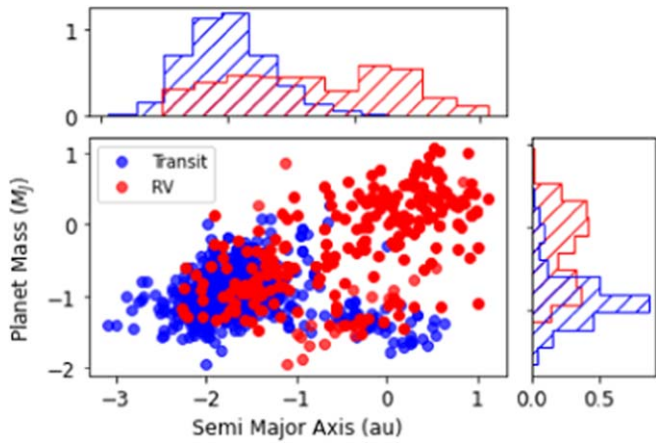


Figure 2. Distribution of planet mass and semimajor axis (on log scale) for the RV and transit planets used in this study. Corresponding histograms are also shown in the top and right panels.

The distribution of planet mass and orbital distance for our sample is shown in Figure 2.

2.5. Abundance Comparison

The elemental abundances derived by different techniques suffer from systematic biases (Blanco-Cuaresma 2019). The abundances for the host stars of CPS and CKS are derived by synthetic spectral fitting using SME (Piskunov & Valenti 2017). On the other hand, the abundances of the HARPS-GTO sample were primarily determined using the equivalent width method using MOOG (Snedden 1973). We wanted to compare whether the elemental abundances obtained by the two different groups have any significant offset or scatter among them. We found 79 stars common between the HARPS-GTO and CPS samples and 56 stars common between the CPS and CKS samples. Figure 3 shows the abundance comparison between the HARPS-GTO versus CPS and CKS versus CPS samples for three different elements: Fe, which is used as a proxy for overall metallicity; Mg, which is an α -peak element; and Mn, which is an iron-peak element. Most stars in the CPS and CKS samples were not only observed using the same telescope and instrumental setup but also analyzed using the same techniques and thus show less spread about the $x = y$ line in Figure 3. Barring few outliers, our analysis indicates that overall abundances determined in three samples using different methods are largely consistent. Since we did not find any significant offset or scatter between our samples, no correction was made for further study.

2.6. Final Sample

The distribution of T_{eff} and $\log g$ for the original HARPS-GTO, CPS, and CKS samples is shown in Figure 1. The original sample includes many evolved stars, mostly subgiants. In this study, we have restricted our analysis to the main-sequence stars, since, for the subgiants, it is difficult to account for non-LTE and evolutionary effects, which can cause mixing in the photospheric abundances. Following the procedure of Brewer & Fischer (2018), we selected stars below the black dashed line (see Figure 1), which represents the main-sequence stars. Thus, our final data consist of 217 planets hosted by 141 stars from the HARPS-GTO sample, 600 stars hosting 1008 planets from the CKS sample, and 227 stars hosting 361

Table 1
Table Listing the Samples from Different Surveys Used in This Paper

Sample	Instrument	Total Stars Observed	Small Planets	Sample after Curation	
				Giant Planets	Super-Jupiters
HARPS-GTO	ESO/HARPS	1111	119	81	17
CKS	Keck/HIRES	1127	934	65	9
CPS	Keck/HIRES	1615	215	117	29

Note. We did not consider the planets hosted by subgiant stars in our sample. The final curated sample consists of only main-sequence stars.

planets in the CPS sample. A detailed description of our final sample is given in Table 1.

3. Analysis and Results

One of the goals of this work is to examine the correlation between the abundance of the host stars with their planet mass and how it relates to the chemical evolution of elements in the galaxy. The knowledge of different elements produced in various stages of GCE can help us understand the observed trends between $[X/\text{Fe}]$ and planet mass. In fact, such trends would be indicative of timescale when planets of different masses were formed. We used regression analysis and Spearman’s coefficients to study the correlation between planet mass and chemical abundances $[X/\text{Fe}]$ of the stellar hosts. In standard linear regression, the presence of outliers can significantly influence the least-squares fit, which approximates the underlying trends between the parameters of interest. Therefore, we used the Huber regression model, which is a robust approach to produce a “weighted” regression line that is less sensitive to outliers. Furthermore, to keep our regression analysis simple, we have not included stars hosting multiple planets belonging to the SP, GP, and/or SJ category. The list of multiplanetary systems comprises 14 stars hosting 34 planets in HARPS-GTO, 24 stars hosting 70 planets in CKS, and 16 stars hosting 42 planets in CPS. The selected PHSs and associated stellar and planetary parameters are given in Table 2. Figure 4 shows the histogram of metallicity distribution of our sample. Clearly, the massive planets ($>0.3 M_J$) are mainly hosted by metal-rich stars, while for the smaller planets ($<0.3 M_J$) there is no specific preference in terms of metallicity of the host stars. The regression trends for various elements are presented in the following subsections.

3.1. α -elements

The α -element abundances of the PHSs can be a proxy to the age of the stars (Delgado Mena et al. 2019). A significant contribution of α -elements comes from SNe II. In this paper, we examine the abundance pattern for four common α -elements (Mg, Si, Ca, and Ti) that were studied in the HARPS, CPS, and CKS samples. Figure 5 shows the variation of α -abundances of host stars with the mass of their planetary companions. The last row in Figure 5 represents the mean abundance of all four α -elements in each sample. The uncertainties associated with the individual abundance measurements are about 0.02–0.05 dex. In the HARPS-GTO case, we find a clear negative correlation for all the α -element abundances with the planet mass. In the case of the CKS sample, which is dominated by small planets, the correlation is

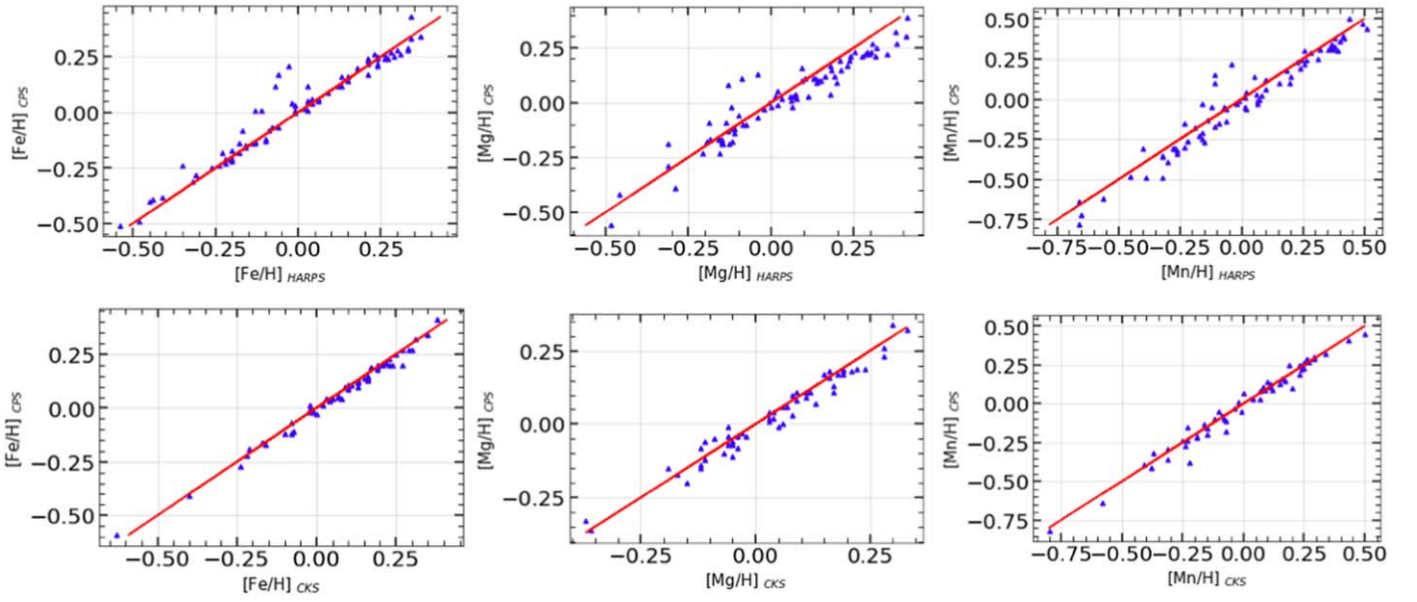


Figure 3. Top row: comparison of elemental abundances of Fe, Mg, and Mn for stars that are common between the CPS and HARPS-GTO samples. Bottom row: comparison of Fe, Mg, and Mn abundance for stars that are common between the CPS and CKS samples. The solid red curve represents the $x = y$ line.

Table 2
Key Parameters of Exoplanet Host Stars Used in This Study

Star ID	Planet Name	R.A.	Decl.	Survey	$M_P(M_J)$	[Fe/H]	[Mg/Fe]	[Si/Fe]	[Ca/Fe]
HD 100777	HD 100777 b	173.9646761	-4.7556922	HARPS-GTO	1.03	0.25	0.04	0.05	-0.035
HD 10180	HD 10180 c	24.4732364	-60.5115264	HARPS-GTO	0.04122	0.08	0.04	0.02	0.012
HD 10180	HD 10180 d	24.4732364	-60.5115264	HARPS-GTO	0.03697	0.08	0.04	0.02	0.012
...									

Note. The entire table is available in machine-readable format. For brevity, only the first three rows and 10 columns are shown here. (This table is available in its entirety in machine-readable form.)

weaker compared to the HARPS-GTO sample. The CPS sample also shows significant negative correlation for all the elements. A strong (weak) correlation implies large (small) Spearman’s rank coefficient and small (large) p -value as shown in Table 3.

Clearly, there is an overall decline of $[\alpha/\text{Fe}]$ with increasing planet mass in all three samples. This can be understood as gradual enrichment of ISM with iron produced in SN Ia, and not necessarily the decline of $[\alpha/\text{H}]$, which can also be seen in Figure A1 in Appendix A. Interestingly, the regression analysis done separately for multiplanetary systems (Appendix B, Figure B1) does not show any significant correlation of $[\alpha/\text{Fe}]$ with the planet mass. Additionally, the overall α -element abundances for this sample are also found to be lower across three mass bins.

3.2. Iron-peak Elements

The significant contribution of iron-peak elements comes from SNe Ia, which occurred at the later stages of GCE compared to SNe II. Again, we analyzed the iron-peak abundance trends for three elements (Cr, Mn, Ni) common for the HARPS-GTO, CKS, and CPS samples and three elements (Co, Cu, Zn) exclusively from the HARPS-GTO sample. Figure 6 (except the last row) and Figure 7 show the iron-peak abundance trends as a function of planet mass. We also find a positive correlation for the Mn abundance with planet mass for all three samples. On the other

hand, the abundance of Zn shows behavior similar to α -peak elements (a strong decreasing trend). This is likely because Zn is also synthesized in core-collapse SNe. Therefore, we see the same effect of GCE in Zn as we see in the α -elements (Kobayashi et al. 2020). For Co, Ni, and Cu, we do not see any significant abundance trends with planet mass. In the case of Cr, we see a negative trend for the HARPS-GTO sample, but we do not see any trend for the CKS and CPS samples. The last row of Figure 6 shows the increasing trend of stellar metallicity ($[\text{Fe}/\text{H}]$) with planet mass, which is a well-established result reported in many similar studies (Fischer & Valenti 2005; Narang et al. 2018).

Overall, the iron-peak elements do not show any significant correlation with planet mass (as listed in Table 3) except for Mn and Zn. In addition, the enrichment of Fe-peak elements with Fe is either increasing (for Mn, Co, Ni, and Cu I) or zero (Cr), as seen in Figure A2, which is in sharp contrast to the trends for α -elements.

3.3. Heavy Elements

Stellar fusion alone cannot produce elements heavier than iron. Most of the heavy elements ($A > 30$) are formed by the neutron-capture processes, which can be broadly classified into slow and rapid processes. The slow process (s -process) takes place when the density of neutrons is low ($n_n \sim 10^8 \text{ cm}^{-3}$), and the successive captures of neutrons happen at a longer timescale ($\sim 10^3 - 10^4 \text{ yr}$; Herwig 2005; Karakas & Lattanzio 2014;

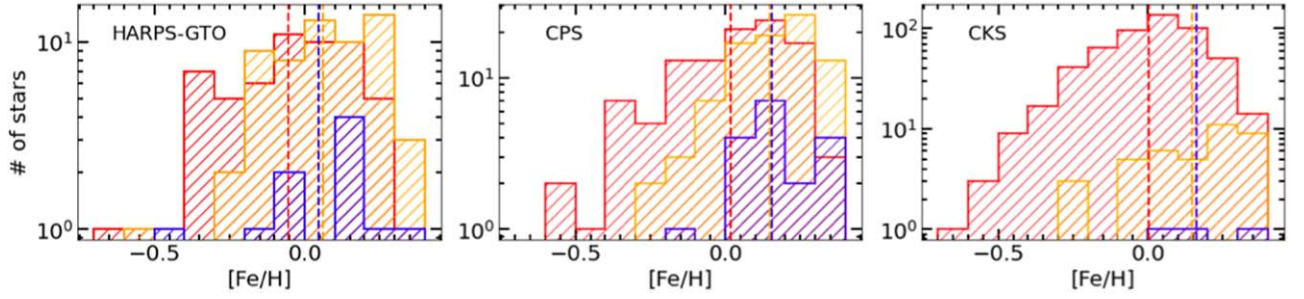


Figure 4. Metallicity distribution for the HARPS-GTO, CKS, and CPS samples. The colors red, yellow, and blue represent small planets, giant planets, and super-Jupiters, respectively. The vertical lines represent the mean of the distribution.

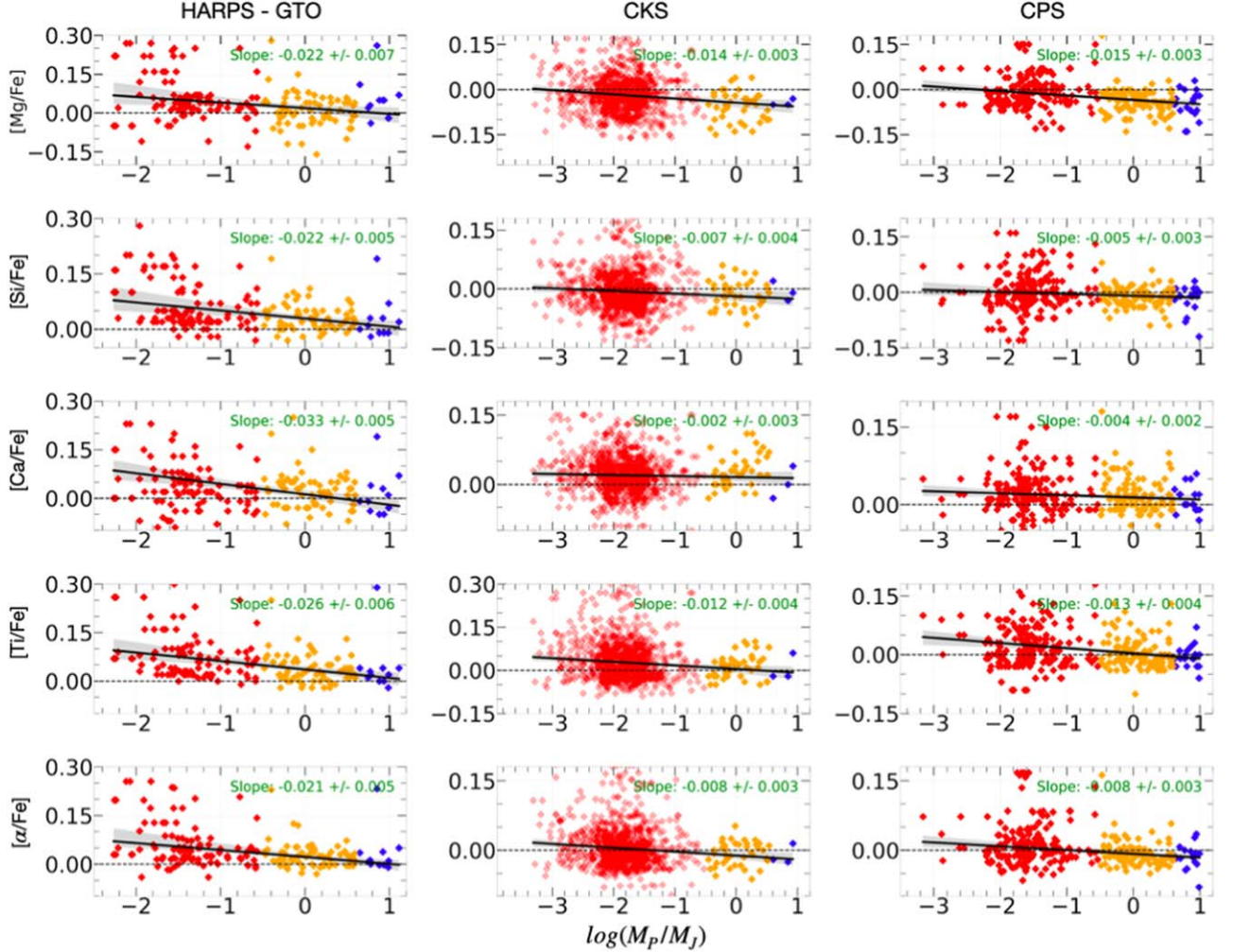


Figure 5. Observed trends for α -element abundances of host stars and planet mass for the HARPS-GTO, CKS, and CPS samples. The colors red, yellow, and blue represent small planets, giant planets, and super-Jupiters, respectively. The black line shows the Huber regression fit, and the gray shaded region represents the 95th percentile confidence interval. The slope value for the best-fit line is shown in each panel. The last row is the arithmetic mean of the α -element abundance from the above four rows.

Frebel 2018; Kobayashi et al. 2020). If the nuclei are unstable, then a β -decay will occur, transforming neutrons to protons (thus increasing atomic number). In the case of the rapid process (r -process), the density of neutrons is higher ($n_n > 10^{22} \text{ cm}^{-3}$); therefore, the timescale is much shorter (\sim few milliseconds to seconds) between the subsequent neutron captures compared to s -process ($\sim 10^3 - 10^4 \text{ yr}$). In addition, since the r -process timescale is much shorter than the β -decay timescales (Baraffe et al. 1992; Cowan et al. 2021), the r -process happens much faster. The GCE

trends for the various heavy elements with Fe are shown in Figure A3. For all the heavy elements, in the region $[\text{Fe}/\text{H}] > -0.5$, we find a gradual decrease in [heavy elements/Fe] abundances with Fe enrichment.

3.3.1. Light s -process Elements

The major production site for the s -process elements is in the He intershell of the asymptotic giant branch (AGB) stars

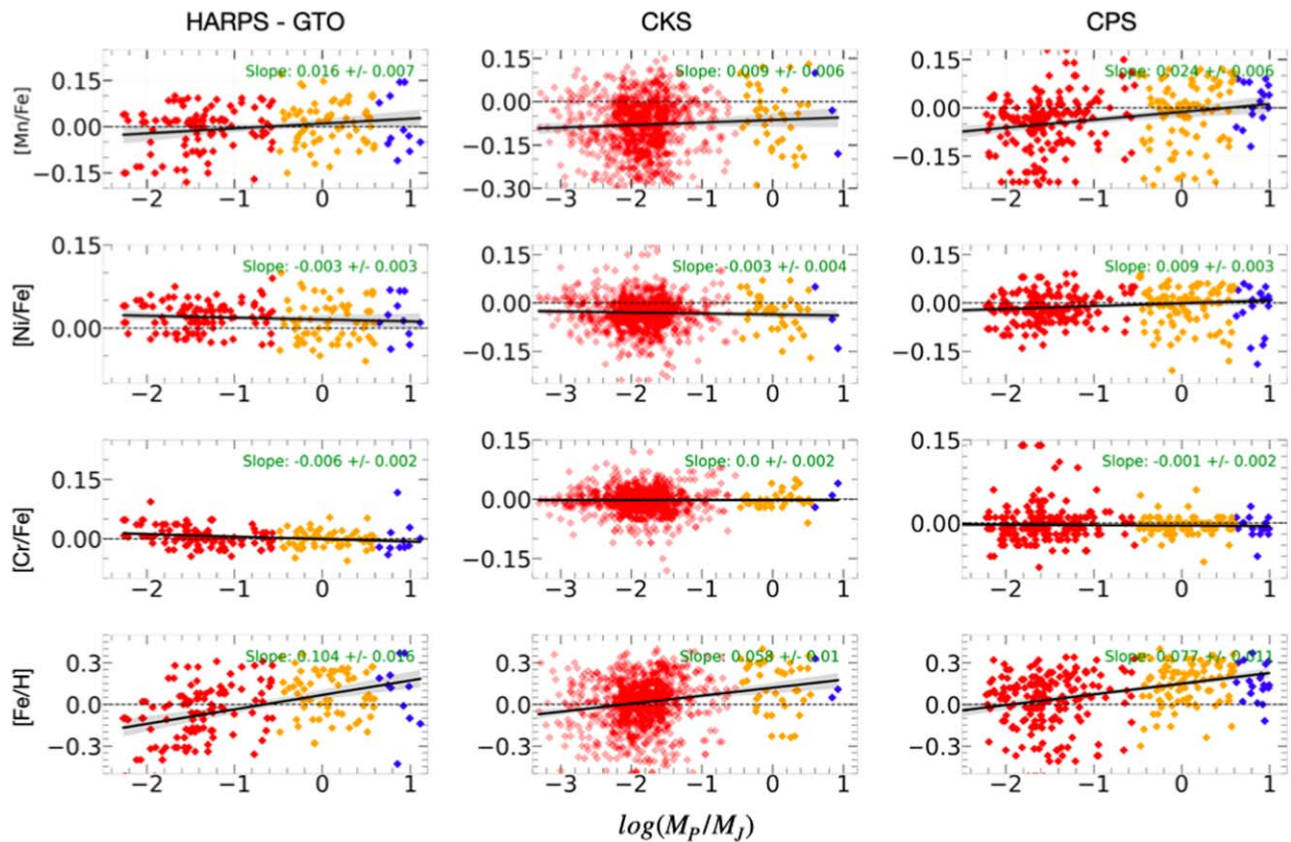


Figure 6. Host star chemical abundances for iron-peak (Mn, Cr, and Ni) elements and metallicity ($[\text{Fe}/\text{H}]$) as a function of planet mass for the HARPS-GTO, CKS, and CPS samples. Symbols and colors are the same as in Figure 5.

Table 3
Spearman's Rank Correlation Coefficient ρ Values Obtained between Elemental Abundance $[\text{X}/\text{Fe}]$ and Planet Mass for the HARPS-GTO, CKS, and CPS Samples

Category	Element	Atomic Number	ρ (p-value)		
			HARPS	CKS	CPS
α -elements	Mg	12	-0.27 (1.93×10^{-4})	-0.10 (2.3×10^{-3})	-0.28 (5.71×10^{-7})
	Si	14	-0.39 (4.02×10^{-8})	-0.10 (3.05×10^{-3})	-0.10 (4.01×10^{-2})
	Ca	20	-0.42 (1.14×10^{-9})	-0.06 (8.02×10^{-2})	-0.13 (1.23×10^{-2})
	Ti	22	-0.45 (1.69×10^{-10})	-0.13 (7.18×10^{-5})	-0.25 (2.84×10^{-6})
	α -avg	...	-0.45 (5.92×10^{-9})	-0.13 (5.661×10^{-5})	-0.25 (6.42×10^{-6})
Iron-peak	Cr	24	-0.22 (2.91×10^{-4})	-0.01 (5.55×10^{-1})	0.00 (9.72×10^{-1})
	Mn	25	0.17 (2.28×10^{-2})	0.08 (3.52×10^{-2})	0.26 (9.37×10^{-7})
	Co	27	-0.08 (1.37×10^{-1})
	Ni	28	-0.08 (2.08×10^{-1})	-0.01 (6.47×10^{-1})	0.12 (4.44×10^{-3})
	Cu	29	-0.14 (4.03×10^{-2})
	Zn	30	-0.39 (3.21×10^{-8})
Light s -process	Sr I	38	0.03 (0.63)
	Y II	39	0.27 (6.99×10^{-5})	0.01 (5.63×10^{-1})	-0.04 (3.11×10^{-1})
	Zr II	40	-0.21 (3.97×10^{-3})
Heavy s -process	Ba II	56	0.17 (2.68×10^{-2})
	Ce II	58	0.06 (3.16×10^{-1})	—	...
	Nd II	60	-0.36 (1.09×10^{-6})
r -process	Eu II	63	-0.37 (1.07×10^{-6})

Note. The values in parentheses represent the p -values associated with the correlation.

(Baraffe et al. 1992; Goswami et al. 2021; Goswami & Goswami 2022). The s -process elements are further categorized based on their atomic masses. Here we studied the abundances for

three light s -process elements (Y, Sr, Zr). The top and bottom rows of Figure 8 show the light s -process abundance trends as a function of planet mass. For Y II and Sr I we do not see any

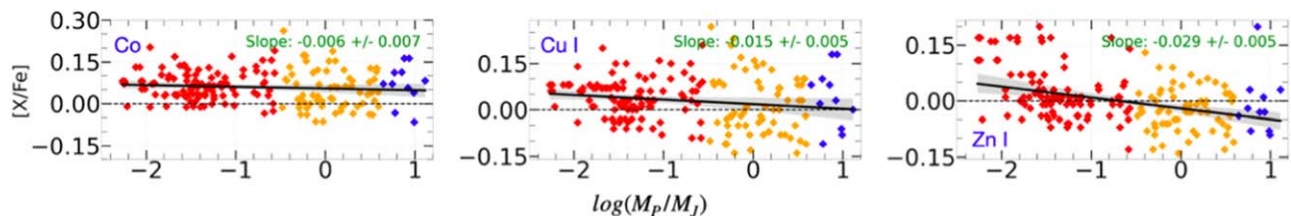


Figure 7. Stellar abundances for iron-peak elements (Co, Cu and Zn) as a function of planet mass exclusively for the HARPS-GTO sample. The Co, Cu, and Zn abundances were not available for the CKS and CPS samples. Once again, the color scheme and the black line representation are the same as in Figure 5.

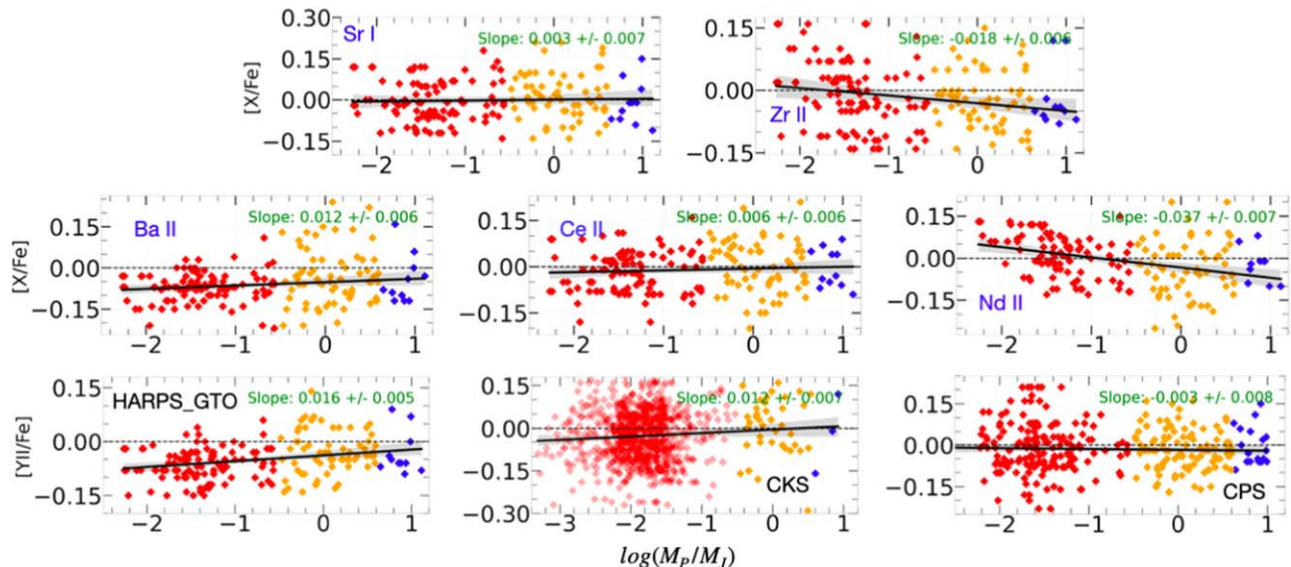


Figure 8. Top row: host star chemical abundances for light s -process elements as a function of planet mass for the HARPS-GTO sample. Middle row: host star chemical abundances for heavy s -process elements as a function of planet mass for the HARPS-GTO sample. The color scheme is the same as that in Figure 5. Bottom row: light s -process element (Y) abundances as a function of planet mass for the HARPS-GTO, CKS, and CPS samples.

significant correlation in our samples, whereas for Zr II we find a negative trend with planet mass as pointed out in Table 3.

3.3.2. Heavy s -process Elements

The three heavy s -process elements analyzed in this work are Ba, Ce, and Nd. The middle row of Figure 8 shows the heavy s -process abundance trends as a function of planet mass. We find that the correlation between Ba II and Ce II abundances and planet mass is weak. On the other hand, Nd shows a strong negative trend as planet mass increases. The behavior of Nd resembles α -elements.

3.3.3. r -process Elements

Although the formation mechanism of r -process elements is a field of active research, with the recent observations of kilonova GW170817, it is possible to explain the Eu abundances solely from neutron-star merger models (van Oirschot et al. 2019). The only pure r -process element known and studied here is Eu from the HARPS-GTO sample. Figure 9 shows the strong negative trend of Eu with planet mass, which looks similar to the α -elements.

4. Discussion

4.1. α -elements: Proxy to Planet Mass and Age

The α -elements primarily formed by SNe II, which happened at the earlier stages of the GCE, while the iron-peak elements are

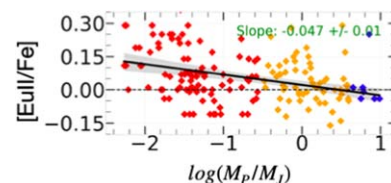


Figure 9. Variation of Eu abundance (r -process element) as a function of planet mass for the HARPS-GTO sample. The color scheme is the same as that in Figure 5.

believed to have formed during SNe Ia, occurring at the later stages of GCE. Relative to iron, the abundances of α -elements and those formed mostly by SNe II in general increase with the age of the star (Nissen 2015; Anders et al. 2018; Bedell et al. 2018; Feuillet et al. 2018; Buder et al. 2019; Delgado Mena et al. 2019). From Figure 5, we see that $[\alpha/\text{Fe}]$ and planet mass have negative slope. In addition, the low-mass planet hosts show larger $[\alpha/\text{Fe}]$ dispersion compared to the parent stars of Jupiters and super-Jupiters (see Section 4.2 for further discussion). One plausible interpretation of such trends is that the low-mass rocky planets have been forming around all generations of stars (old as well as young), while the high-mass giant planets likely formed around younger stars when the ISM was sufficiently enriched with iron-peak elements. The same reasoning must apply to the multiplanetary systems hosting at least one low-mass planet and one high-mass planet such as Jupiters or super-Jupiters. As shown in Figure B1 in Appendix B, the slope between α -element abundance and planet mass is nearly an order of

magnitude smaller compared to the corresponding slopes in Figure 5. This implies that multiplanetary systems accompanying at least one high-mass planet are clearly α -deficient and therefore younger. This would not be the case for multiplanetary systems hosting only the small planets.

Since the iron-peak elements are formed at later stages of GCE, it suggests a similar formation time line for the hosts of giant planets and possibly super-Jupiters, if core accretion was the dominant mechanism. Moreover, the abundance of iron-peak elements scales in the same way as the abundance of iron [Fe/H]. Thus, the trends for iron-peak elements with planet mass are nearly positive or zero, as expected except for Zn, which shows a strong negative trend similar to α -elements. The anomalous behavior of Zn is also seen in several studies (e.g., Bisterzo et al. 2004; Mikolaitis et al. 2017; Delgado Mena et al. 2019). Zn is found to increase with age, as it is also synthesized in core-collapse SNe, and thus follows the GCE trends similar to α -elements (Kobayashi et al. 2020). We also see a positive trend for Mn as planet mass increases. Mn is produced mostly in SNe Ia (Nomoto et al. 1997; Kobayashi et al. 2006), and this trend indicates that statistically massive planet hosts are Mn-rich, and the presence of Mn in the host star may be crucial in the formation of giant planets. Interestingly, the GCE effect is also strong for [Mn/Fe], even for the field stars, as evident from Figure A2. However, that alone cannot explain the relatively large slope of [Mn/Fe] versus planet mass among iron-peak elements seen in Figure 6. The yields for Ni are quite similar during SNe Ia and SNe II (Nomoto et al. 2013; Mikolaitis et al. 2017); thus, we expect a flat trend with planet mass, which is also seen observationally. In line with GCE, the absence of any significant trend in iron-peak elements with planet mass independently suggests that production of most iron-peak elements coevolved with Fe. But more importantly, the later enrichment of the ISM with Fe and iron-peak elements, as the trends indicate, could be an important ingredient for the formation of high-mass planets.

For the heavy elements, the trends with planet mass can also be explained by the hypothesis discussed above. In the case of Eu, which is an r -process element, it is largely formed through neutron-star mergers (Drout et al. 2017; Côté et al. 2018). These merger events predate the timescales of SNe Ia (Skúladóttir & Salvadori 2020; Reggiani et al. 2021). Further, studies have also shown that Eu abundance increases with age (Snaith et al. 2015; Delgado Mena et al. 2019) similar to α -elements. In our analysis, we find that Eu elemental abundance decreases as planet mass increases, a behavior similar to that of α -elements. The decrease of [Eu/Fe] with planet mass further strengthens our results and supports our hypothesis that exoplanet host stars with planet mass $>0.3 M_J$ could indeed be younger than SP hosts.

The s -process elements are primarily produced in low-mass AGB stars; thus, their contribution is expected to increase with time. The light s -process (Sr, Y, Zr) elements also show trends similar to iron-peak elements. Their trends for chemical abundances have a negative correlation with age (≤ 8 Gyr) as shown by other studies (e.g., Battistini & Bensby 2016; Delgado Mena et al. 2019), which is expected, as their production time line is similar to that of the iron-peak elements. For heavy s -process element Ba, we see a positive slope with planet mass, but the trends are opposite for Nd, with Nd showing a strong negative trend with planet mass similar to Eu. This is because even though Nd is considered as a heavy

s -process element, only about 56% of it is formed via the s -process (Arlandini et al. 1999; Bisterzo et al. 2016). The remaining Nd is produced by the r -process, predating the timescales of the s -process. Thus, in light of GCE, the α -element abundance seems a good proxy for the planet mass. One possible implication of this finding could be that stars hosting small planets have been forming through all epochs, while the formation of stars hosting giant planets and super-Jupiters happened in a later epoch when the ISM was sufficiently enriched by the iron and iron-peak elements.

4.2. Independent Age Analysis

The negative correlation between α -elements and planet mass presented in Section 3 indicates that stellar hosts of giant planets are probably younger. To corroborate our result, we took the independent age estimates of the HARPS-GTO, CPS, and CKS samples from Delgado Mena et al. (2019), Brewer et al. (2016), and Brewer & Fischer (2018), respectively. In these studies, the stellar ages were determined using the isochrone fitting technique requiring effective temperature (T_{eff}) and luminosity (L), which were obtained from photometric and spectroscopic studies. For the HARPS-GTO sample, the ages were estimated using GAIA DR2 parallaxes and PARSEC isochrones (Bressan et al. 2012), while for the CPS and CKS samples the ages were determined by Yonsei–Yale isochrones (Demarque et al. 2004) and Dartmouth Stellar Evolution isochrones (Dotter et al. 2008). Although the individual age estimates will vary depending on the choice of model, they will not impact the underlying statistical trends, as these models do not have any significant systematics (Delgado Mena et al. 2019).

The age distribution of our samples divided into three mass bins is shown in Figure 10. We see that the host stars of giant planets ($M_p > 0.3 M_J$) and super-Jupiters are younger compared to stars hosting smaller planets. For example, the median age (in Gyr) of SP, GP, and SJ hosts is 6.40, 4.30, and 5.23 for the HARPS-GTO sample and 6.58, 4.62, and 4.3 for the CPS and CKS samples, respectively. For PHSs in the HARPS-GTO sample, Delgado Mena et al. (2019; see their Figure 7) have found a positive correlation between $[\alpha/\text{Fe}]$ abundances and stellar age. This, combined with the decrease of negative slope between $[\alpha/\text{Fe}]$ and planet mass found in this work, further lends independent support to our inference that stellar systems harboring massive planets could be younger.

Further, within the giant planet population, there is an observed paucity of hot Jupiters around old stars. To explain the dearth of old stars hosting massive and hot planets, Hamer & Schlaufman (2019) have argued that the tidal interaction between the host star and the planet can cause the planet to spiral into the star. Older stars will lose their hot Jupiters if this tidal infall timescale is relatively short. However, the tidal infall timescale (based on Equation (4) in Hamer & Schlaufman 2019) for a Jupiter-like planet around a Sun-like star for orbital periods $\gtrsim 7$ days can be as long as the main-sequence lifetime of these stars. The tidal infall timescales are even longer for planets less massive than Jupiter. Only giant planets with $M_p > 2 M_J$ and orbital period < 5 days have tidal infall timescale much shorter than 1 Gyr. Hence, tidal infall might be playing a key role, but it alone cannot explain the lack of hot giant planets around older stars (see also Narang et al. 2022, under review).

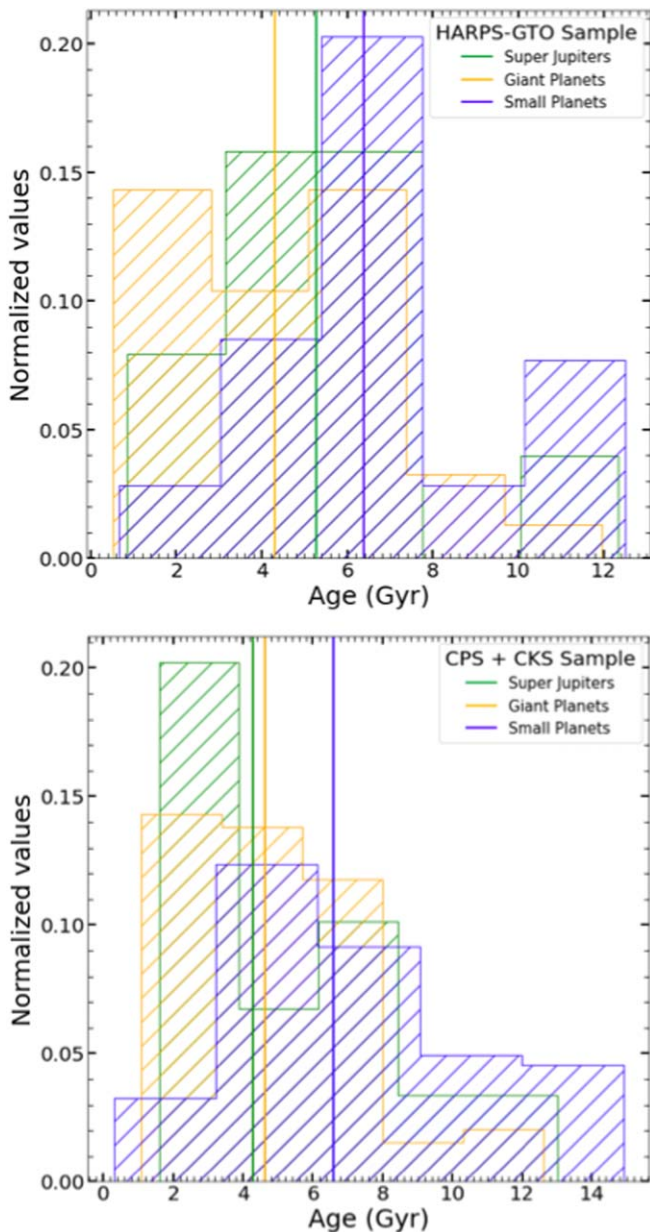


Figure 10. Age distribution of PHSs derived using isochrone fitting. The vertical lines represent the median for each of the distributions.

Abundance scatter or dispersion is another measure of implicit spread in stellar ages. With the chemical evolution of the galaxy, the dispersion in elemental abundance, especially $[\alpha/\text{Fe}]$, is expected to increase. We refer to the abundance spread seen in Figures 5 and 6. This spread is further quantified in Figure 11, where we show the heat maps for the 1σ scatter in the abundance distribution of the stellar hosts. From Figure 11, the 1σ scatter for α -element abundances is much more pronounced for the small PHSs than the Jupiter and super-Jupiter hosts. Also, the scatter in the iron-peak elements, except for Mn, is relatively smaller than the α -elements in all three samples. The large scatter in the α -element abundances implies a large dispersion in ages of stars hosting small planets. This means that small planets started forming early in Our galaxy, when $[\alpha/\text{Fe}]$ was high, and continued to form in later generations of stars, when $[\alpha/\text{Fe}]$ has declined. On the contrary, the abundance distribution of stars hosting Jupiter

analog and super-Jupiters has small scatter and hence similar age, indicating that the massive planets belong to a later generation of stars, represented by overall low $[\alpha/\text{Fe}]$ and increased iron-peak element abundance. Note that the overall scatter seen in Figures 5 and 6 is much larger than the error in abundance determination of individual stars, which is typically 0.02–0.05 dex.

4.3. GCE and Formation of Giant Planets

Results from Section 3 clearly establish a link between the abundance of iron and iron-peak elements and the giant planets. Among existing theories, gravitational instability is proposed as a preferred method for the formation of giant planets beyond the snow line (Boss 1997; Mayer et al. 2002). Additionally, Kratter et al. (2010) showed that for a runaway gravitational instability of the disk to happen, the gas cooling time has to be shorter than the Keplerian shearing timescale. One could speculate that at large distances (\sim tens of au) from the star the radiative losses from the metals in a protoplanetary disk could possibly contribute to the cooling of the gas during the nascent stage. However, scores of directly imaged planets and brown dwarfs found in wider orbits have not shown any marked dependence on the stellar metallicity (Swastik et al. 2021).

The close-by gas giants detected by transit and RV surveys are expected to form via core accretion processes (Pollack et al. 1996; Matsuo et al. 2007; Birnstiel et al. 2016; Owen & Murray-Clay 2018; Drzaskowska et al. 2022). The GCE trends for α - and iron-peak elements in Appendix A (Figures A1–A3) show that in the region $[\text{Fe}/\text{H}] > -0.5$ $[\alpha/\text{Fe}]$ decreases with the enrichment of $[\text{Fe}/\text{H}]$, but for iron-peak elements the trends are mostly flat or increasing with $[\text{Fe}/\text{H}]$. Therefore, with the enrichment of Fe in ISM, the content of iron-peak elements scales much faster with Fe compared to the α -peak abundances. The fact that the gas giants are known to be formed from a metal-rich protoplanetary disk is a natural consequence of the large addition of iron-peak elements.

To form a gas giant via the core accretion mechanism, two significant steps must be followed. The first is the formation of a solid mass embryo with a mass of about $\sim 10 M_{\oplus}$ in the protoplanetary disk by numerous collisions and coagulation of the planetesimals (for more comprehensive details, please refer to Drzaskowska et al. 2022). The second is the rapid accretion of gas from the protoplanetary disk before the gas and dust are completely dissipated (Rice & Armitage 2003; Birnstiel et al. 2016; Drzaskowska et al. 2022). To accrete and form a gaseous envelope around the solid core, the core must grow relatively faster (3–10 Myr; Matsuo et al. 2007; Ayliffe & Bate 2012; Emsenhuber et al. 2021; Drzaskowska et al. 2022). Whether a protoplanet will end up like a rocky planet or a gas giant will depend on the amount of material present in the protoplanetary disk (Alibert et al. 2005). The gas giant planet formation requires the core to build faster to outdo the gas dissipation rate so that the gas is not entirely depleted by the time the massive core ($\sim 10 M_{\oplus}$) is formed. Although protoplanetary disks were massive during the early phase of GCE, the refractory α -elements alone would have contributed to the formation of the core. By the time the core formed, most of the gas in the disk would dissipate, leading to a preferential formation of rocky planets. However, as the galaxy chemically evolved, the ISM was enriched in both α - and iron-peak elements coming from the SNe Ia. This additional enrichment would propel the growth of grains, pebbles, planetesimals, and, finally, the core

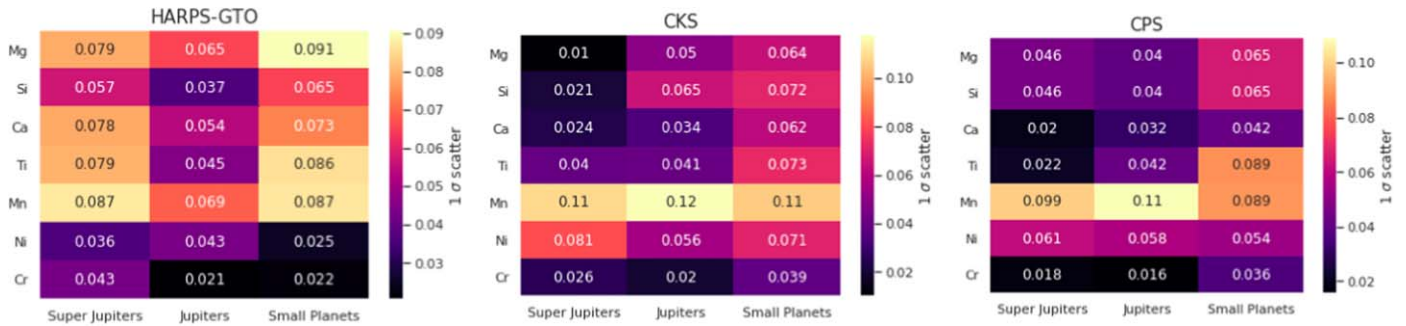


Figure 11. Heat map of 1σ scatter from Figures 5 and 6 for the abundance dispersion of the host stars of small planets, Jupiters, and super-Jupiters. A linear detrending was applied to the original abundance data to compute the 1σ scatter for each mass bin.

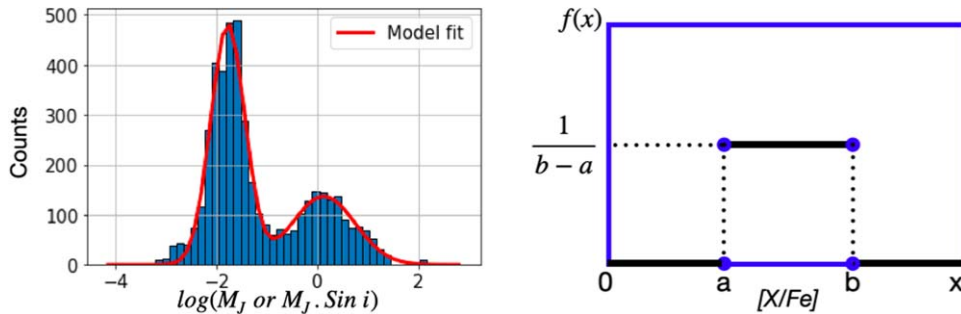


Figure 12. Left: the observed distribution of exoplanet mass (in log scale) taken from the NASA exoplanet archive. Right: a uniform distribution assumed for α -element abundances of PHSs.

(Emsenhuber et al. 2021; Draskowska et al. 2022). Since the chemically enriched material fuels the growth of the core quickly reaching the critical mass, the disk will have sufficient gas left to accrete onto the surface of the core to form the gas giants (Matsuo et al. 2007; Ayliffe & Bate 2012; Emsenhuber et al. 2021; Draskowska et al. 2022). Thus, the delayed enrichment of ISM by SNe Ia created pathways for the formation of gas giants, which seems consistent with the core accretion process.

4.4. Biases and Statistical Validity of Our Results

Exoplanet host stars selected from various transits and RV surveys could suffer from different detection and selection biases. The transit method, for example, is primarily sensitive to planets orbiting close to the star with near-edge-on configuration. The RV method, on the other hand, is suitable to detect giant planets at large orbital distances (see, e.g., Figure 2). Since the RV precision is adversely affected by stellar activity and line broadening mechanisms, the highly active and fast-rotating stars are usually excluded from the RV surveys, keeping the focus largely on the main-sequence dwarfs. However, to our knowledge no study exists that links the chemical composition of stars to stellar activity and/or rotation. Therefore, it is very unlikely that possible biases in RV/transit search would impact the chemical analysis of the exoplanet hosting stars. As reported in Section 3, the stellar abundance trends with planet mass are similar and consistent with GCE for all three samples, regardless of the search method.

Further, to ensure that our results are not biased owing to low number statistics or random correlations in the abundances, a Monte Carlo test was carried out. We attempted to reproduce the correlations obtained in Section 3 by using simulated planet

masses and abundances. Since the trends for α -elements were most robust, we used them as a case study for this analysis. For our simulations, we constructed a bimodal function describing the observed planet mass distribution as shown in the left panel of Figure 12. The apparent mass distribution of confirmed exoplanets has two peaks, one near $0.01 M_J$ and another at $1 M_J$. The intrinsic mass distribution of exoplanets could be different from the apparent mass distribution, but we discount any selection effects since they are hard to quantify (Malhotra 2015).

For abundances, we assumed a uniform distribution, bound by a rectangular window function shown in the right panel of Figure 12. The lower and upper bounds for the abundance distributions in each sample are taken at the 3σ cutoff on either side of the observed distribution mean of the averaged α -abundances plotted in the last row of Figure 5.

For each simulation run, we randomly draw 500 samples from the assumed distributions of planet masses and abundances. We then calculate the slope of the best-fit line between the planet masses and abundances. The goal is to check how often the observed slope is reproduced in a reasonably large numerical experiment, with underlying abundance distribution assumed to be uniform. The simulation was repeated 100,000 times, and the final histograms of slopes are shown in Figure 13. For the HARPS-GTO sample, the observed slopes for all the elements are significantly far from the mean of the numerical slopes, suggesting that observed trends are highly improbable owing to chance outcome. In fact, none of the trials produced results that matched the observed slopes, thus rendering the probability of observed trends arising from random occurrence extremely low ($\leq 10^{-5}$). Similarly, for the CKS and CPS samples, the observed slopes for Mg, Si, and Ti are also significantly away

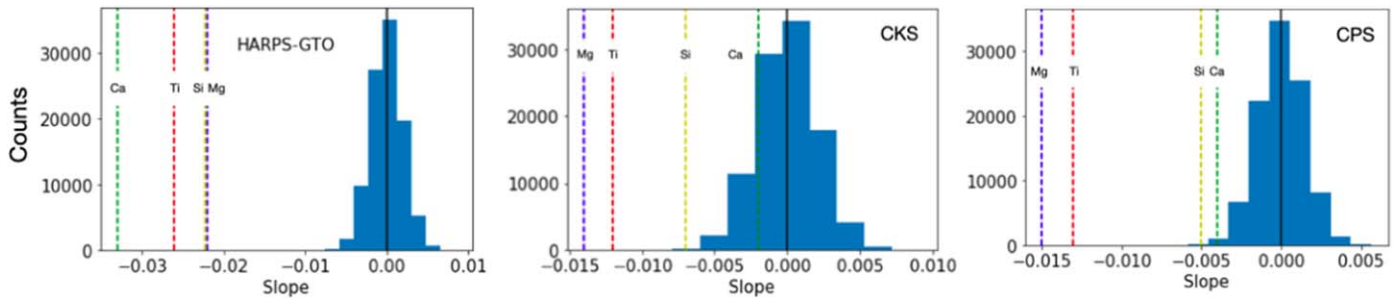


Figure 13. The distribution of numerical slope (between α -element abundances of host star and planet mass) generated from Monte Carlo simulations for the HARPS-GTO, CKS, and CPS samples. The solid black line represents the mean of the distribution, and the dotted color lines represent the measured slope from Figure 5.

from the mean of the numerical distribution, with the exception of Ca, which is only about 1σ (CKS) and 3σ (CPS) away. Generally, this analysis suggests that the observed α -element trends obtained in Section 3 cannot be generated by simple randomness, and these trends are also not due to low number statistics. Therefore, the planet–abundance pattern observed in a finite sample of exoplanet host stars must be a correct manifestation of the underlying population.

5. Summary and Conclusions

Exoplanet properties are intimately connected to the properties of their stellar hosts. In this work we studied the chemical abundances of planets hosting stars for planets in different mass bins. We analyzed the abundances of 17 elements belonging to different classes based on their formation mechanism and evolution of chemical history of the galaxy. We used data from well-known exoplanet search programs, namely, HARPS-GTO, CKS, and CPS, and planetary mass from the NASA exoplanet catalog. Our analysis includes 968 PHSs, which are discovered by both the transit and RV methods. Here we present a summary of our results:

1. We find that for all the α -elements, which are mainly produced in SNe II, there is an unambiguous negative slope with planet mass for all three samples used in this study, showing that stars hosting small planets are clearly α -rich compared to stars harboring giant planets and super-Jupiters.
2. We find a positive correlation for Mn and near-zero correlation for the iron-peak elements for almost all the cases with planet mass. Since iron-peak elements are primarily formed during SNe Ia and followed the same scaling as iron, their surface composition $[X/Fe]$ in stellar hosts remains mostly the same, regardless of the planet mass.
3. For the r -process elements, Eu, which is mainly produced by neutron-star mergers, happened at much earlier stages of GCE (earlier than SNe Ia), and thus the $[Eu/Fe]$ versus planet mass trend is similar to that of α -elements.
4. The s -process elements are primarily produced in AGB stars and are formed at much later stages of the GCE (after SN Ia enrichment). We expected their trends to follow iron-peak elements. However, we find that Nd shows a significant negative trend with planet mass. This could be because a significant amount of Nd is produced by the r -process.
5. Our abundance analysis of exoplanet host stars shows two specific trends with planet mass: a distinct negative

slope for α -elements including Eu, and a near-zero slope for most iron-peak elements. Seen in the context of GCE, these results imply that stellar systems with small planets may have started forming early in the evolutionary history of our Galaxy, whereas the emergence of high-mass planetary systems had to wait until the ISM was sufficiently enriched.

6. To validate our findings, we compare the stellar ages estimated from the isochrone fitting. Our independent age analysis also shows that host stars of massive gas giant planets are indeed statistically younger than the stars hosting low-mass planets.
7. Compared to their low-mass counterparts, we also find a relatively small scatter in the abundance distribution of stellar hosts of high-mass planets. This is compatible with the younger age and temporal offset in the formation scenario of Jupiters and super-Jupiters.
8. Our sample of multiplanetary systems hosting at least one low-mass and one high-mass planetary companion do not show any correlation between $[\alpha/Fe]$ and planet mass. In addition, their overall $[\alpha/Fe]$ abundance across all three mass bins is also lower. This, too, suggests the possibility that such multiplanetary systems are younger.

In conclusion, we have analyzed the elemental abundances of a large sample (968) of PHSs, connecting the planet formation process to the evolution of the chemical enrichment of the ISM. The detailed abundances of exoplanet host stars are largely consistent with the GCE. From the observed trends between stellar abundances and planet mass, we conclude that the low-mass planets may have been formed during all epochs of star formation, while the giant planets are formed around chemically enriched stars that are relatively young.

To strengthen these findings, the future high-resolution spectroscopic surveys should target a larger sample of exoplanet hosting stars, determining their chemical abundances uniformly and homogeneously. More theoretical and experimental work is required to further understand the importance of chemical abundance, especially the role that iron-peak elements play in the formation and growth of dust grains, pebbles, and planetesimals in the astrophysical environment.

We would like to thank the anonymous referee for the useful comments and suggestions that helped us in improving the manuscript. This work has made use of (a) the NASA Exoplanet Database, which is run by the California Institute of Technology under an Exoplanet Exploration Program contract with the National Aeronautics and Space Administration; (b) the European Space Agency (ESA) space mission

Gaia, the data from which were processed by the Gaia Data Processing and Analysis Consortium (DPAC); (c) the exoplanet.eu database developed and maintained by the exoplanet TEAM. C.S. would like to thank E. Delgado Mena for providing us with the list of exoplanet hosting stars for the HARPS-GTO sample. C.S. would also like to thank P. P. Goswami and Pallavi Saraf for the insightful discussion on formation of heavy elements. C.S. would also thank Anirban Dutta for the discussions on supernovae and its contribution to various element formation.

Software: Astropy (Astropy Collaboration et al. 2013), Scikit-learn (Pedregosa et al. 2011), Topcat (Taylor 2005),

Scipy (Virtanen et al. 2020), Matplotlib (Hunter 2007), numpy (Harris et al. 2020).

Appendix A Elemental Abundances $[X/Fe]$ as a Function of $[Fe/H]$

The $[X/Fe]$ versus $[Fe/H]$ trends for the sample of exoplanet host stars studied in this paper are shown in Figures A1–A3. In the case of α -elements we see the $[X/Fe]$ trend to be decreasing with $[Fe/H]$, while for iron-peak elements we see a variety of trends with $[Fe/H]$. The overall trends seen in these figures are consistent with the standard GCE model. The PHSs primarily lie in the metal-rich regime, as seen below.

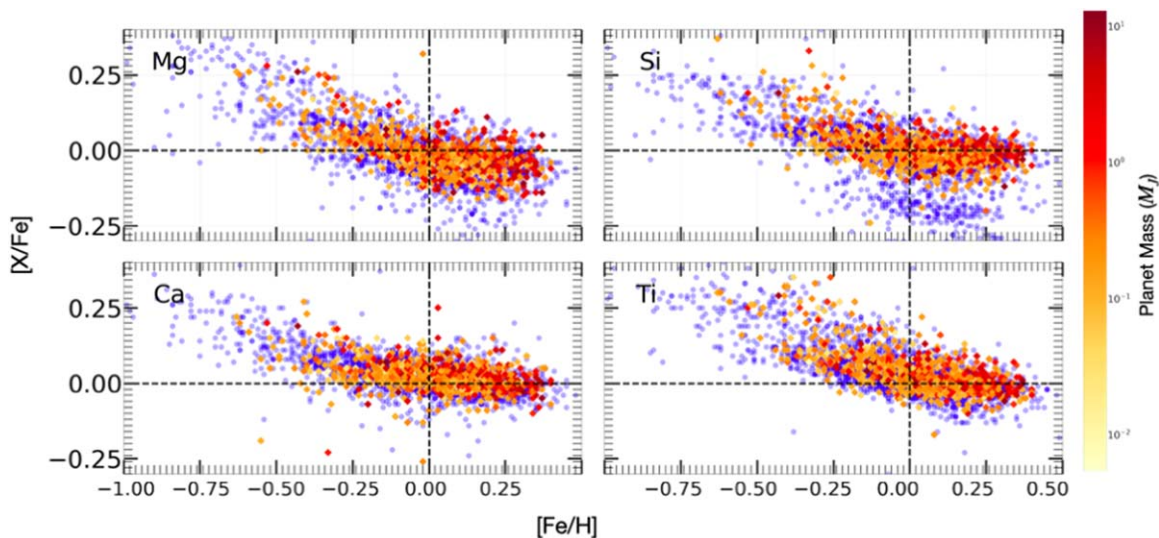


Figure A1. Abundance ratios $[X/Fe]$ vs. $[Fe/H]$ for α -elements for stars belonging to all three samples: HARPS-GTO, CKS, and CPS. The blue circles represent SWPs, while the color bar represents stars hosting planets of different mass.

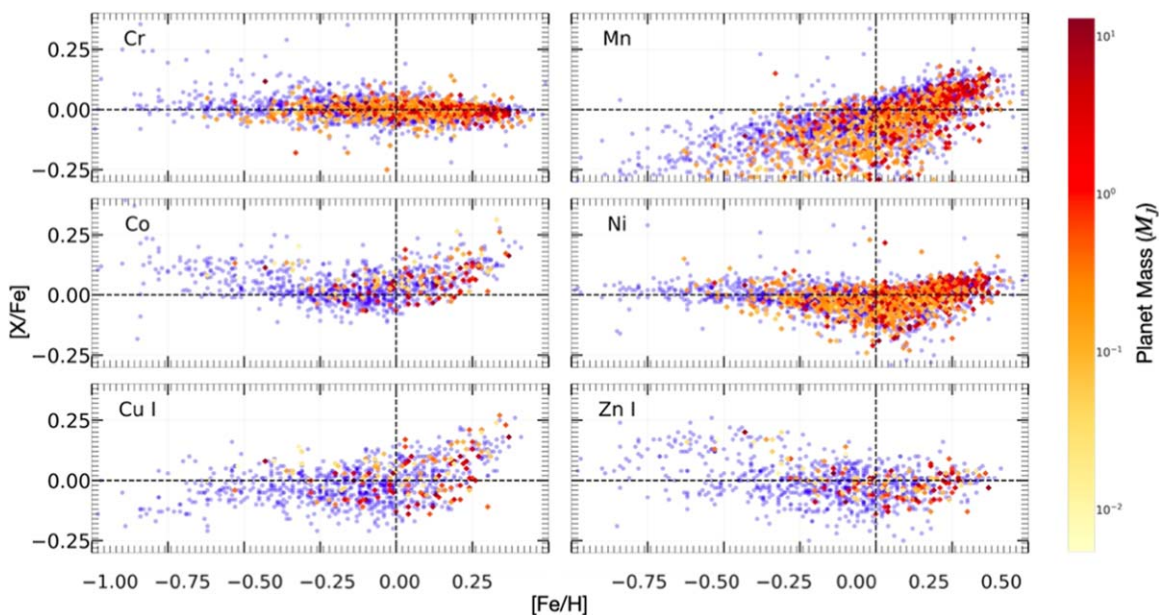


Figure A2. Abundance ratios $[X/Fe]$ vs. $[Fe/H]$ for iron-peak elements for stars belonging to all three samples: HARPS-GTO, CKS, and CPS. The blue circles represent SWPs, while the color bar represents stars hosting planets of different mass.

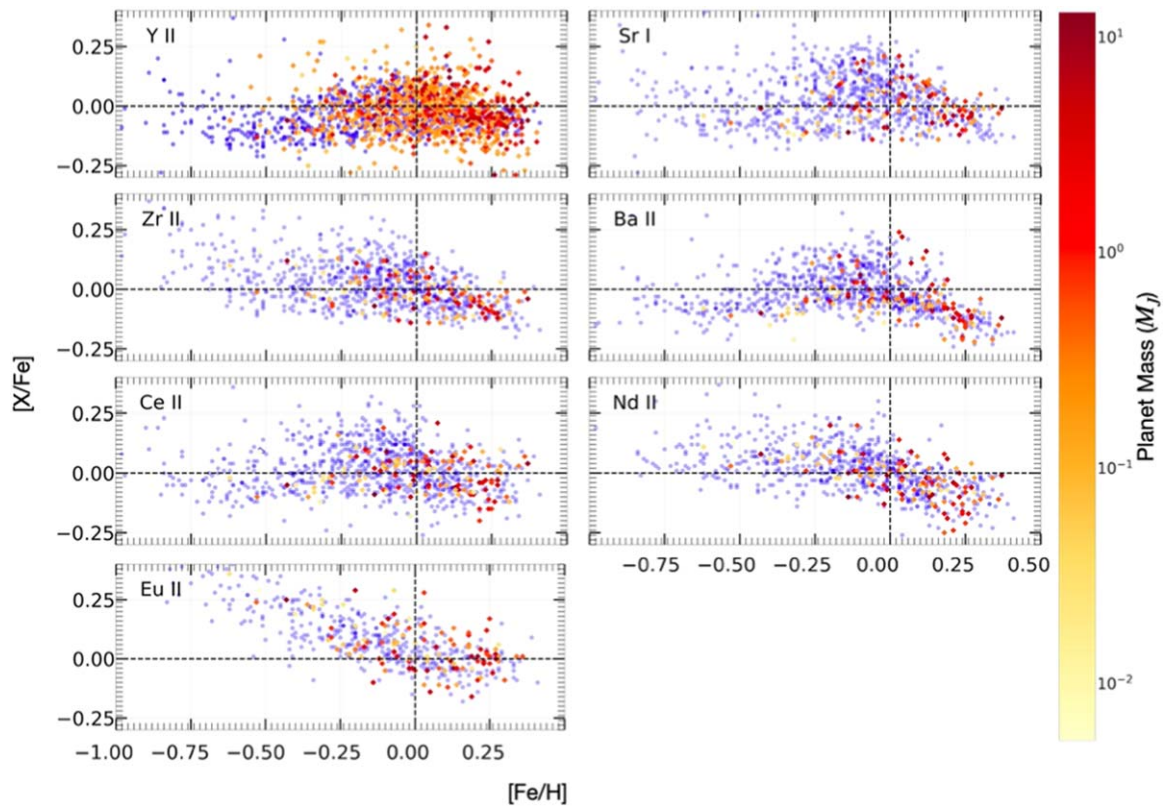


Figure A3. Abundance ratios $[X/Fe]$ vs. $[Fe/H]$ for heavy elements ($A > 30$) for stars belonging to all three samples: HARPS-GTO, CKS, and CPS. The blue circles represent SWPs, while the color bar represents stars hosting planets of different mass.

Appendix B

α -element Abundance for the Multiplanetary Systems

For the subsample of multiplanetary systems excluded from the analysis in Section 3, we do not find noticeable correlation

between the α -element abundance and the planet mass (see Figure B1). This indicates that the multiplanetary systems that host at least one giant or a supergiant are also recently formed.

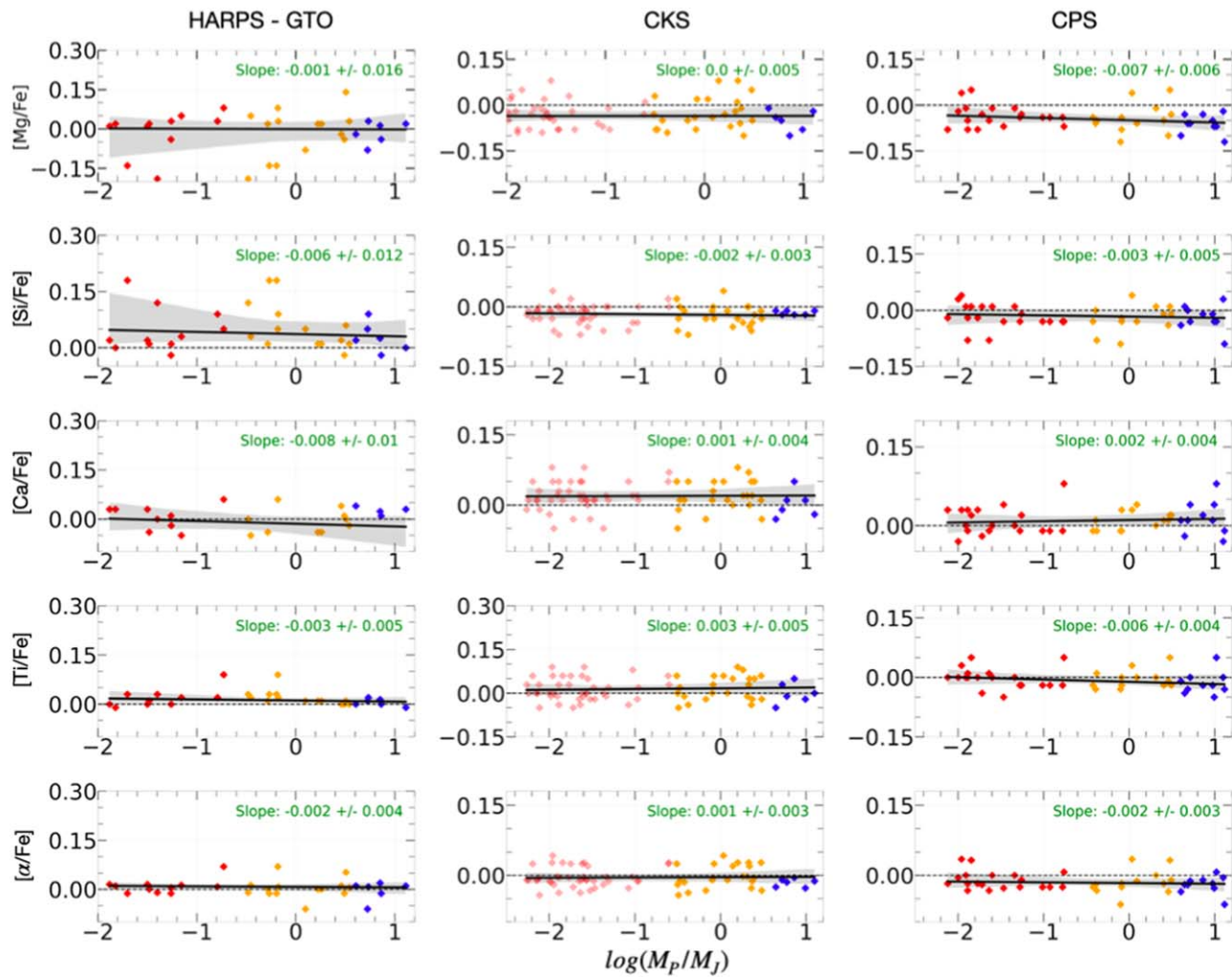





Figure B1. α -element abundances as a function of planet mass for the multiplanetary systems that host at least one planet each in low-mass and Jupiter- and/or super-Jupiter-mass regimes. The last row is the arithmetic mean of the α -element abundance from the above four rows.

ORCID iDs

C. Swastik  <https://orcid.org/0000-0003-1371-8890>
 Ravinder K. Banyal  <https://orcid.org/0000-0003-0799-969X>
 Mayank Narang  <https://orcid.org/0000-0002-0554-1151>
 P. Manoj  <https://orcid.org/0000-0002-3530-304X>
 T. Sivarani  <https://orcid.org/0000-0003-0891-8994>
 S. P. Rajaguru  <https://orcid.org/0000-0003-0003-4561>
 Athira Unni  <https://orcid.org/0000-0001-6093-5455>
 Bihan Banerjee  <https://orcid.org/0000-0001-8075-3819>

References

- Adibekyan, V. 2019, *Geosc*, **9**, 105
 Adibekyan, V. Z., Santos, N. C., Sousa, S. G., et al. 2012a, *A&A*, **543**, A89
 Adibekyan, V. Z., Santos, N. C., Sousa, S. G., & Israelian, G. 2011, *A&A*, **535**, L11
 Adibekyan, V. Z., Sousa, S. G., Santos, N. C., et al. 2012b, *A&A*, **545**, A32
 Akeson, R. L., Chen, X., Ciardi, D., et al. 2013, *PASP*, **125**, 989
 Alibert, Y., Mordasini, C., Benz, W., & Winisdoerffer, C. 2005, *A&A*, **434**, 343
 Alibés, A., Labay, J., & Canal, R. 2001, *A&A*, **370**, 1103
 Anders, F., Chiappini, C., Santiago, B. X., et al. 2018, *A&A*, **619**, A125
 Arlandini, C., Käppeler, F., Wisshak, K., et al. 1999, *ApJ*, **525**, 886
 Astropy Collaboration, Robitaille, T. P., Tollerud, E. J., et al. 2013, *A&A*, **558**, A33
 Ayliffe, B. A., & Bate, M. R. 2012, *MNRAS*, **427**, 2597
 Baraffe, I., El Eid, M. F., & Prantzos, N. 1992, *A&A*, **258**, 357
 Battistini, C., & Bensby, T. 2016, *A&A*, **586**, A49
 Bedell, M., Bean, J. L., Meléndez, J., et al. 2018, *ApJ*, **865**, 68
 Bertran de Lis, S., Delgado Mena, E., Adibekyan, V. Z., Santos, N. C., & Sousa, S. G. 2015, *A&A*, **576**, A89
 Birstiel, T., Fang, M., & Johansen, A. 2016, *SSRv*, **205**, 41
 Bisterzo, S., Gallino, R., Pignatari, M., et al. 2004, *Mem. Soc. Astron. Italiana*, **75**, 741
 Bisterzo, S., Travaglio, C., Wiescher, M., et al. 2016, *JPhCS*, **665**, 012023
 Blanco-Cuaresma, S. 2019, *MNRAS*, **486**, 2075
 Blanco-Cuaresma, S., Soubiran, C., Heiter, U., & Jofré, P. 2014, *A&A*, **569**, A111
 Borucki, W. J., Koch, D. G., Basri, G., et al. 2011, *ApJ*, **736**, 19
 Boss, A. P. 1997, *Sci*, **276**, 1836
 Bressan, A., Marigo, P., Girardi, L., et al. 2012, *MNRAS*, **427**, 127
 Brewer, J. M., & Fischer, D. A. 2018, *ApJS*, **237**, 38
 Brewer, J. M., Fischer, D. A., Valenti, J. A., & Piskunov, N. 2016, *ApJS*, **225**, 32
 Brugamyer, E., Dodson-Robinson, S. E., Cochran, W. D., & Sneden, C. 2011, *ApJ*, **738**, 97
 Bruntt, H., Basu, S., Smalley, B., et al. 2012, *MNRAS*, **423**, 122
 Buchhave, L. A., Bizzarro, M., Latham, D. W., et al. 2014, *Natur*, **509**, 593
 Buder, S., Lind, K., Ness, M. K., et al. 2019, *A&A*, **624**, A19
 Chen, J., & Kipping, D. 2017, *ApJ*, **834**, 17
 Costa Silva, A. R., Delgado Mena, E., & Tsantaki, M. 2020, *A&A*, **634**, A136
 Côté, B., Fryer, C. L., Belczynski, K., et al. 2018, *ApJ*, **855**, 99
 Cowan, J. J., Sneden, C., Lawler, J. E., et al. 2021, *RvMP*, **93**, 015002
 Delgado Mena, E., Adibekyan, V., Santos, N. C., et al. 2021, *A&A*, **655**, A99
 Delgado Mena, E., Adibekyan, V. Z., Figueira, P., et al. 2018, *PASP*, **130**, 094202
 Delgado Mena, E., Moya, A., Adibekyan, V., et al. 2019, *A&A*, **624**, A78
 Delgado Mena, E., Tsantaki, M., Adibekyan, V. Z., et al. 2017, *A&A*, **606**, A94
 Demarque, P., Woo, J.-H., Kim, Y.-C., & Yi, S. K. 2004, *ApJS*, **155**, 667
 Dong, S., Zheng, Z., Zhu, Z., et al. 2014, *ApJL*, **789**, L3
 Dotter, A., Chaboyer, B., Jevremović, D., et al. 2008, *ApJS*, **178**, 89
 Drazkowska, J., Bitsch, B., Lambrechts, M., et al. 2022, arXiv:2203.09759
 Drouot, M. R., Piro, A. L., Shappee, B. J., et al. 2017, *Sci*, **358**, 1570
 Ecuivillon, A., Israelian, G., Santos, N. C., et al. 2004, *A&A*, **426**, 619
 Edvardsson, B., Andersen, J., Gustafsson, B., et al. 1993, *A&A*, **500**, 391
 Emsenhuber, A., Mordasini, C., Burn, R., et al. 2021, *A&A*, **656**, A70
 Everett, M. E., Howell, S. B., Silva, D. R., & Szkody, P. 2013, *ApJ*, **771**, 107
 Feuillet, D. K., Bovy, J., Holtzman, J., et al. 2018, *MNRAS*, **477**, 2326
 Fischer, D. A., & Valenti, J. 2005, *ApJ*, **622**, 1102
 Fleming, S. W., Mahadevan, S., Deshpande, R., et al. 2015, *AJ*, **149**, 143
 Frebel, A. 2018, *ARNPS*, **68**, 237
 Gonzalez, G. 1997, *MNRAS*, **285**, 403
 Goswami, P. P., & Goswami, A. 2022, *A&A*, **657**, A50
 Goswami, P. P., Rathour, R. S., & Goswami, A. 2021, *A&A*, **649**, A49
 Hamer, J. H., & Schlaufman, K. C. 2019, *AJ*, **158**, 190
 Harris, C. R., Millman, K. J., van der Walt, S. J., et al. 2020, *Natur*, **585**, 357
 Haywood, M., Di Matteo, P., Lehnert, M. D., Katz, D., & Gómez, A. 2013, *A&A*, **560**, A109
 Herwig, F. 2005, *ARA&A*, **43**, 435
 Hinkel, N. R., Timmes, F. X., Young, P. A., Pagano, M. D., & Turnbull, M. C. 2014, *AJ*, **148**, 54
 Howard, A. W., Johnson, J. A., Marcy, G. W., et al. 2010, *ApJ*, **721**, 1467
 Hunter, J. D. 2007, *CSE*, **9**, 90
 Johnson, J. A., Aller, K. M., Howard, A. W., & Crepp, J. R. 2010a, *PASP*, **122**, 905
 Johnson, J. A., Howard, A. W., Marcy, G. W., et al. 2010b, *PASP*, **122**, 149
 Johnson, J. A., Petigura, E. A., Fulton, B. J., et al. 2017, *AJ*, **154**, 108
 Karakas, A. I., & Lattanzio, J. C. 2014, *PASA*, **31**, e030
 Kobayashi, C., Karakas, A. I., & Lugaro, M. 2020, *ApJ*, **900**, 179
 Kobayashi, C., Umeda, H., Nomoto, K., Tominaga, N., & Ohkubo, T. 2006, *ApJ*, **653**, 1145
 Kratter, K. M., Matzner, C. D., Krumholz, M. R., & Klein, R. I. 2010, *ApJ*, **708**, 1585
 Laughlin, G., & Adams, F. C. 1997, *ApJL*, **491**, L51
 Lin, D. N. C., Bodenheimer, P., & Richardson, D. C. 1996, *Natur*, **380**, 606
 Lo Curto, G., Mayor, M., Benz, W., et al. 2010, *A&A*, **512**, A48
 Malhotra, R. 2015, *ApJ*, **808**, 71
 Matsuo, T., Shibai, H., Ootsubo, T., & Tamura, M. 2007, *ApJ*, **662**, 1282
 Matteucci, F., & Francois, P. 1989, *MNRAS*, **239**, 885
 Matteucci, F., Spitoni, E., Recchi, S., & Valiante, R. 2009, *A&A*, **501**, 531
 Mayer, L., Quinn, T., Wadsley, J., & Stadel, J. 2002, *Sci*, **298**, 1756
 Mayor, M., Marmier, M., Lovis, C., et al. 2011, arXiv:1109.2497
 Mayor, M., Pepe, F., Queloz, D., et al. 2003, *Msngr*, **114**, 20
 Mayor, M., & Queloz, D. 1995, *Natur*, **378**, 355
 Mikolaitis, Š., de Laverny, P., Recio-Blanco, A., et al. 2017, *A&A*, **600**, A22
 Mulders, G. D. 2018, in *Handbook of Exoplanets*, ed. H. Deeg & J. Belmonte, Vol. 153 (Cham: Springer),
 Murray, N., Chaboyer, B., Arras, P., Hansen, B., & Noyes, R. W. 2001, *ApJ*, **555**, 801
 Narang, M., Manoj, P., Furlan, E., et al. 2018, *AJ*, **156**, 221
 NASA Exoplanet Science Institute 2020, Planetary Systems Table, IPAC,
 Nissen, P. E. 2015, *A&A*, **579**, A52
 Nomoto, K., Iwamoto, K., Nakasato, N., et al. 1997, *NuPhA*, **621**, 467
 Nomoto, K., Kobayashi, C., & Tominaga, N. 2013, *ARA&A*, **51**, 457
 Owen, J. E., & Murray-Clay, R. 2018, *MNRAS*, **480**, 2206
 Pedregosa, F., Varoquaux, G., Gramfort, A., et al. 2011, *JMLR*, **12**, 2825
 Petigura, E. A., Howard, A. W., Marcy, G. W., et al. 2017, *AJ*, **154**, 107
 Petigura, E. A., Marcy, G. W., Winn, J. N., et al. 2018, *AJ*, **155**, 89
 Pinsonneault, M. H., DePoy, D. L., & Coffee, M. 2001, *ApJL*, **556**, L59
 Piskunov, N., & Valenti, J. A. 2017, *A&A*, **597**, A16
 Pollack, J. B., Hubickyj, O., Bodenheimer, P., et al. 1996, *Icar*, **124**, 62
 Reggiani, H., Schlaufman, K. C., Casey, A. R., Simon, J. D., & Ji, A. P. 2021, *AJ*, **162**, 229
 Rice, W. K. M., & Armitage, P. J. 2003, *ApJL*, **598**, L55
 Santos, N. C., Israelian, G., & Mayor, M. 2001, *A&A*, **373**, 1019
 Santos, N. C., Israelian, G., & Mayor, M. 2004, *A&A*, **415**, 1153
 Santos, N. C., Mayor, M., Bonfils, X., et al. 2011, *A&A*, **526**, A112
 Skúladóttir, Á., & Salvadori, S. 2020, *A&A*, **634**, L2
 Snaith, O., Haywood, M., Di Matteo, P., et al. 2015, *A&A*, **578**, A87
 Sneden, C. 1973, *ApJ*, **184**, 839
 Suárez-Andrés, L., Israelian, G., González Hernández, J. I., et al. 2016, *A&A*, **591**, A69
 Suárez-Andrés, L., Israelian, G., González Hernández, J. I., et al. 2017, *A&A*, **599**, A96
 Swastik, C., Banyal, R. K., Narang, M., et al. 2021, *AJ*, **161**, 114
 Tautvaišienė, G., Mikolaitis, Š., & Drazdauskas, A. 2022, *ApJS*, **259**, 45
 Taylor, M. B. 2005, in *ASP Conf. Ser. 347, Astronomical Data Analysis Software and Systems XIV*, ed. P. Shopbell, M. Britton, & R. Ebert (San Francisco, CA: ASP), 29
 Udry, S., & Santos, N. C. 2007, *ARA&A*, **45**, 397
 Valenti, J., & Fischer, D. 2008, in *ASP Conf. Ser. 384, 14th Cambridge Workshop on Cool Stars, Stellar Systems, and the Sun*, ed. G. van Belle (San Francisco, CA: ASP), 292
 van Oirschot, P., Nelemans, G., Pols, O., & Starmenburg, E. 2019, *MNRAS*, **483**, 4397
 Virtanen, P., Gommers, R., Oliphant, T. E., et al. 2020, *NatMe*, **17**, 261
 Viswanath, G., Narang, M., Manoj, P., Mathew, B., & Kartha, S. S. 2020, *AJ*, **159**, 194
 Wilson, R. F., Cañas, C. I., Majewski, S. R., et al. 2022, *AJ*, **163**, 128
 Wright, J. T., Veras, D., Ford, E. B., et al. 2011, *ApJ*, **730**, 93